AEROSPACE REPORT NO.
TR-2009(8550)-10

Airborne Particulate Sampling in Environmental Control Systems

15 July 2009

De-Ling Liu and Kenneth T. Luey
Space Materials Laboratory
Physical Sciences Laboratories

Prepared for:

Space and Missile Systems Center
Air Force Space Command
483 N. Aviation Blvd.
El Segundo, CA 90245-2808

Authorized by: Engineering and Technology Group

This report was submitted by The Aerospace Corporation, El Segundo, CA 90245-4691, under Contract No. FA8802-09-C-0001 with the Space and Missile Systems Center, 483 N. Aviation Blvd., El Segundo, CA 90245. It was reviewed and approved for The Aerospace Corporation by G. F. Hawkins, Principal Director, Space Materials Laboratory; and D. C. Marvin, Principal Director, Research and Program Development Office. David E. Davis was the project officer for the Mission-Oriented Investigation and Experimentation (MOIE) program.

This report has been reviewed by the Public Affairs Office (PAS) and is releasable to the National Technical Information Service (NTIS). At NTIS, it will be available to the general public, including foreign nationals.

This technical report has been reviewed and is approved for publication. Publication of this report does not constitute Air Force approval of the report's findings or conclusions. It is published only for the exchange and stimulation of ideas.

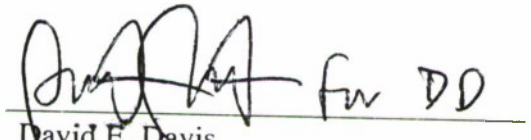

David E. Davis
SMC/EA

REPORT DOCUMENTATION PAGE

Form Approved
OMB No. 0704-0188

1. REPORT DATE (*DD-MM-YYYY*)	2. REPORT TYPE	3. DATES COVERED (*From - To*)
15-07-2009		

4. TITLE AND SUBTITLE

Airborne Particulate Sampling in Environmental Control Systems

5a. CONTRACT NUMBER
FA8802-09-C-0001

5b. GRANT NUMBER

5c. PROGRAM ELEMENT NUMBER

6. AUTHOR(S)

De-Ling Liu and Kenneth T. Luey

5d. PROJECT NUMBER

5e. TASK NUMBER

5f. WORK UNIT NUMBER

7. PERFORMING ORGANIZATION NAME(S) AND ADDRESS(ES)

The Aerospace Corporation
Physical Sciences Laboratories
El Segundo, CA 90245-4691

8. PERFORMING ORGANIZATION REPORT NUMBER

TR-2009(8550)-10

9. SPONSORING / MONITORING AGENCY NAME(S) AND ADDRESS(ES)

Space and Missile Systems Center
Air Force Space Command
483 N. Aviation Blvd.
El Segundo, CA 90245

10. SPONSOR/MONITOR'S ACRONYM(S)
SMC

11. SPONSOR/MONITOR'S REPORT NUMBER(S)

12. DISTRIBUTION/AVAILABILITY STATEMENT

Approved for public release; distribution unlimited.

13. SUPPLEMENTARY NOTES

14. ABSTRACT

HEPA-filtered purge air supplied by an environmental control system (ECS) is used to protect encapsulated spacecraft from particulate contamination. Therefore, it is imperative to acquire representative air samples from the ECS ducts in order to ensure that the air cleanliness requirements per mission specifications are achieved. Based on well-established work involving particle transport in the literature, this report quantitatively examines the particle sampling efficiency with respect to the sampling apparatus and conditions relevant to the routine ECS air quality verification procedures during launch processing operations.

In brief, the low overall transmission efficiency indicates that the measurement of 5 μm and larger particles routinely done in the ECS air sampling procedures is highly unlikely to provide valid data due to the significant particle sampling losses. On the other hand, the measurement of 0.5-μm particles serves as a better indicator for the purge air quality verification owing to nearly 100% transmission efficiency for this particle size range.

15. SUBJECT TERMS

ECS, Air sampling, Isokinctic sampling, Aerosol sampling

16. SECURITY CLASSIFICATION OF:			17. LIMITATION OF ABSTRACT	18. NUMBER OF PAGES	19a. NAME OF RESPONSIBLE PERSON
					De-Ling Liu
a. REPORT	b. ABSTRACT	c. THIS PAGE	Leave blank	37	19b. TELEPHONE NUMBER *(include area code)*
UNCLASSIFIED	UNCLASSIFIED	UNCLASSIFIED			(310)336-0062

Acknowledgments

This work was supported under Air Force Mission-Oriented Investigation and Experientation Program and The Aerospace Corporations' Independent Research and Development Program.

Contents

Figures

Tables

1. Introduction

After spacecraft encapsulation, a conditioned air purge is continuously flown from an environmental control system (ECS) into the payload fairing (PLF) in order to minimize both particulate and molecular contamination resulting from ambient air intrusion. It is important to ensure that the airborne particulate concentration of ECS air has met the cleanliness requirements through air sampling.

The ECS consists mainly of (1) an air filtration unit, which is equipped with charcoal and HEPA filters to remove airborne organic molecular and particulate contaminants, respectively; and (2) flex ducts that deliver filtered clean air to the PLF. During launch processing, the ECS air typically flows at 190–300 lb/min (2139–4010 cfm) in circular flex ducts of 8, 10, or 12 inch in diameter (20.3, 25.4, or 30.5 cm), hence, the resulting air velocities could be in the range of 16–58 m/s.

Before the ECS air is connected to the payload fairing, the air cleanliness level is verified by taking air samples from the end of a flex duct using a sampling probe, tubing, and a particle detection instrument (an optical particle counter, OPC, is normally used). To ensure that a representative aerosol* sample, in terms of concentration and size distribution, is collected from unidirectional moving air streams, isokinetic sampling is commonly employed. To achieve isokinetic conditions, the air at the sampling probe entrance has to be withdrawn at the same velocity as the approaching air in the duct. As a result, the inner diameter of an isokinetic sampling probe needs to be small, ranging from 2.8 to 5.8 mm, in order to reach the same air velocity as the ECS air in the duct when the sampling flowrate is fixed at 1 cfm (to OPC). Because of this difference in diameters between an ECS duct and a sampling probe, only a very small fraction of the ECS air (2.5 to 5%) is sampled from a small cross section of the duct (surface area ratio ~10^{-4}) via the isokinetic process. Figure 1 presents an overview of the isokinetic sampling conditions for the ECS air under typical ground processing environments.

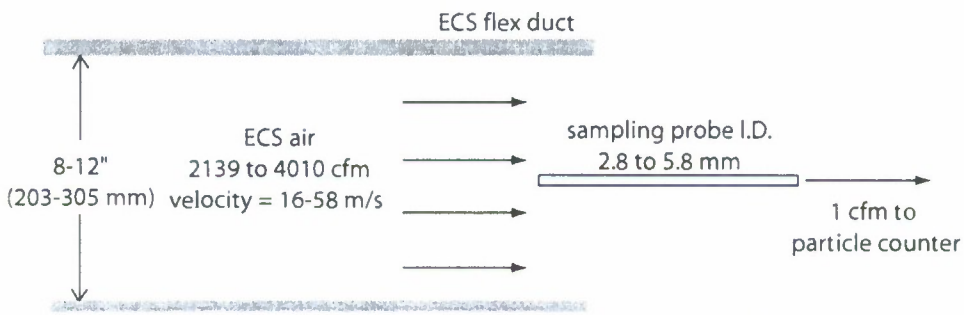

Figure 1. Schematic of ECS air sampling (sideview) using isokinetic sampling probe located in the center of the circular ECS duct.

* Aerosol: solid or liquid particles suspended in a gas.

In light of only a very small fraction of ECS air being sampled in the air cleanliness verification process, the goal of this report is to gain insights into the validity and the potential measurement errors with respect to the aerosol sampling practice. The knowledge of aerosol transport and sampling is employed to examine the particle sampling efficiency associated with the sampling apparatus and conditions relevant to the routine ECS air quality verification procedures during launch processing operations. These insights are necessary because the airflow conditions associated with the launch pad ECS are quite extreme compared to, for example, the atmospheric environment or the range of air flow conditions addressed by appendices in FED-STD-209E. The ECS mass flow rates and the associated air velocities are very high compared to the sampling rate of the particle measuring instrument. Additionally, safety concerns for ECS air sampling require the use of tubing up to 10 feet long with one or more turns. All these factors can contribute to the uncertainty of particle sampling accuracy.

In this report, quantitative estimates of potential particle losses under realistic ECS air sampling scenarios are provided. The report also gives general guidelines to minimize particle losses associated with the sampling procedures based on the physics of particle transport behaviors. In Section 2, a brief overview of aerosol sampling is presented, based on existing literature, which describes incremental particle losses in each component of a typical air sampling system. In the subsequent sections, sampling losses at each of those system components are evaluated in detail. Section 3 addresses factors affecting aspiration efficiency at the probe inlet, and Section 4 examines sampling losses in the tubing. Section 5 presents recommendations for improved airborne particle sampling under high-velocity scenarios.

2. Overview of Aerosol Sampling

To determine the airborne particle concentration in an air stream, an aerosol sample must be withdrawn and delivered into a particle measurement device, or collected on a filter. Ideally, the collected sample should contain the same particle size distribution and concentration as the air in the original environment, and be unaffected by the sampling process.

An aerosol sampling train, which is employed to measure particle concentrations in air, normally consists of a sampling probe, a sample transfer line (or a sampling tube), and a particle measurement device or a filter. The accuracy of the sampled aerosols is determined by the extent of particle losses (1) at the sampling probe, and (2) in the sample transfer line. Figure 2 illustrates these two important aspects of aerosol sampling. (For illustrative purpose only, Figure 2 does not include bends in the sample transfer line.)

The concept of sampling efficiency is used to characterize the fraction of airborne particles in the approaching air streams delivered to the particle measurement device through the sampling probe and the sample transfer line. The overall sampling or transmission efficiency, $\eta_{overall}$, is given by:

$$\eta_{overall} = \eta_{probe} \times \eta_{trans,line}$$

$$= (\eta_{asp} \times \eta_{trans,probe}) \times \eta_{trans,line}, \qquad (1)$$

where

η_{probe}: the probe or inlet efficiency; the fraction of ambient aerosols that are delivered to the sample transfer line by the probe.

$\eta_{trans,line}$: the transmission efficiency of the sampling line; the fraction of particles that are transported from the end of sampling probe and through the entire sample transfer line.

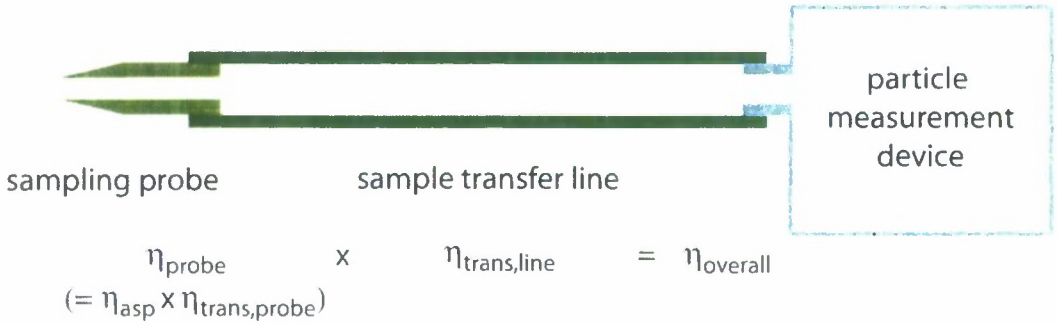

Figure 2. Schematic of an aerosol sampling train (not to scale).

η_{asp}: the aspiration efficiency; the ratio of particle concentration sampled at the probe entrance to that in the approaching air stream from which the sample is taken.

$\eta_{trans,probe}$: the transmission efficiency of the sampling probe; the fraction of aspirated particles that are transmitted through the sampling probe to the rest of the sampling system.

All of these sampling efficiencies are a function of the particle size. Figure 2 also indicates the corresponding efficiencies with respect to the aerosol sampling system.

When significant particles losses (i.e., low sampling efficiency) occur at the sampling probe and within the sample transfer line, the particle counting results received by the measurement device will underestimate the true aerosol concentrations, therefore giving the false impression that the air is clean in terms of airborne particulate levels.

Aerosol sampling in an ECS duct is a unique scenario where unidirectional air runs at extremely high velocities. In this work, the focus is on aerosol sampling issues with respect to ECS air quality certifications during launch processing. In this report, we provide quantitative estimates of potential particle losses under realistic ECS air sampling scenarios. In addition, recommendations are made to minimize particle losses associated with the sampling procedures, based on the physics of particle transport and deposition behavior. The following two sections will be devoted to discussions of particle sampling losses associated with sampling probes and sampling lines, respectively.

3. Aspiration of Particles at a Sampling Probe

Withdrawing a representative aerosol sample into a sampling probe inlet is not a trivial task. For example, the following factors all play a role in determining the extent of particle losses at a sampling inlet:

1. orientation of the sampling probe with respect to the approaching gas stream;
2. velocity and direction of the approaching gas stream;
3. velocity of the sampling flow at the sampling probe inlet;
4. geometry and shape of the sampling probe inlet;
5. particle aerodynamic diameter.

To collect representative aerosol samples into a sampling inlet, all of these factors have to be taken into account simultaneously. These factors will be addressed qualitatively in Subsection 3.1 and quantitatively in Subsection 3.3.

3.1 Isokinetic Sampling

The procedure of isokinetic sampling is to ensure that a *representative* sample of airborne particles enters a sampling probe from a moving air stream. Sampling is isokinetic when the sampling probe is aligned parallel to the air streamlines, and the average air velocity* through the sampling probe inlet equals the free-stream air velocity approaching the inlet (Hinds, 1999; Baron and Willeke, 2001; FED-STD-209E, 1992). Any procedures that deviate from isokinetic sampling will result in biased aerosol sampling and unreliable measurement data. The following discussion addresses how the factors mentioned previously contribute to sampling errors.

3.1.1 Sampling Probe Orientation; the relative magnitude of air velocities at the sampling inlet and In the free stream air

In practice, the orientation of the sampling probe will be aligned parallel to the air streamlines, and the probe geometry (i.e., inner diameter) will be tailored to produce nearly identical air velocity at the sampling probe inlet as in the free-stream air velocity to achieve isokinetic sampling. Subsection 3.2 will elaborate on this, and a sample calculation will be provided.

---

* spatial average over the cross-sectional area of the duct. In turbulent flow regime, the average air velocity is very close to the air velocity measured in the center of the duct.

3.1.2 Shape of a Sampling Probe Inlet

The inlet of an isokinetic sampler is normally a thin-walled, sharp-edged probe or tube in order to minimize air streamline distortion at the sampling probe inlet (Hinds, 1999; Baron and Willeke, 2001; Belyaev and Levin, 1974). The airstream distortion as a result of sampling probe wall thickness is illustrated in Figure 3. The eddy currents in the vicinity of sampling probe inlet are responsible for particle losses due to deposition. Research has shown that a decrease in aspiration efficiency is strongly correlated with the increasing sampling probe thickness (Belyaev and Levin, 1972). Therefore, the sampling process using a thick-walled probe will give rise to biased data and cannot represent the true airborne particle size distribution and concentration. The definition of a "thin-walled" probe is discussed in Subsection 3.3.

3.1.3 Particle Aerodynamic Diameter

At the sampling inlet, gravitational settling and particle inertia are the two dominant particle deposition mechanisms responsible for particle losses. As a result, representative aerosol sampling becomes increasingly challenging with respect to larger particle size.

Here is a brief introduction of the two major particle deposition mechanisms at the inlet:

(1) Gravitational settling

Airborne particles are removed from air and fall onto surfaces because gravity pulls them downward. Large particles are more strongly influenced by gravity than small particles, and therefore they are more easily removed from the airstream. This is expressed by the particle settling velocity, which is proportional to the square of the particle diameter, d_p^2.

$$V_s = \frac{\rho_p d_p^{\,2} g C_c}{18\mu}, \tag{2}$$

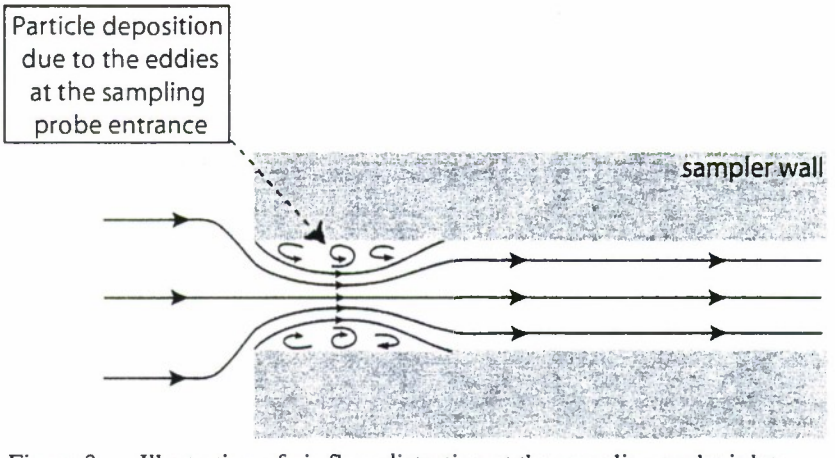

Figure 3 Illustration of air flow distortion at the sampling probe inlet when using a thick-walled aerosol sampler.

where

V_s: particle settling velocity

ρ_p: particle density

d_p: aerodynamic particle diameter

g: acceleration of gravity

μ: air dynamic viscosity; 1.8×10^{-5} kg/m·s at 20°C

C_c: Cunningham slip correction factor* (the values of C_c are 1.033 and 1.333 for 5 μm and 0.5 μm particles, respectively), which is a function of particle size and is defined as:

$$C_c = 1 + \frac{\lambda}{d_p}\left[2.514 + 0.800\exp\left(-0.55\frac{d_p}{\lambda}\right)\right], \quad (3)$$

where λ is mean free path of surrounding gas molecules ($\lambda = 0.066$ μm at 1 atm and 20°C) .

Assuming unit density, for instance, the settling velocities for 1 μm and 10 μm particles are 3.50×10^{-3} cm/s and 0.305 cm/s, respectively.

(2) Inertial impaction

Owing to their inertia, airborne particles may not follow the air streamlines well, and consequently become deposited onto surfaces of sampling probe entrance as a result of inertial impaction. Particle inertia can be a valid sampling concern for large particles traveling in high air flow velocities. To characterize particle inertia in flowing air streams, a dimensionless Stokes number (*Stk*) is calculated, which is defined as

$$Stk = \frac{\rho_p d_p^2 U_o C_c}{18\mu L}, \quad (4)$$

where

Stk: a dimensionless parameter used to characterize particle inertia in moving air streams

* The Cunningham correction factor is used to account for the fact that small particles (<1 μm) settle faster than predicted by Stokes's law where the relative velocity of the gas at the particle surface is zero. When the particle size approaches the mean free path of gas molecules, a nonzero relative velocity of the gas at the surface of particles (so-called "slip" conditions) occurs so that the drag force predicted by Stokes's law is reduced.

U_o: free stream air flow velocity

L: characteristic dimension of the system

The characteristic dimension in the scenario of ECS air sampling is the sampling probe I.D.

As shown in Eq. (4), particle inertia in flowing air* is characterized by properties of the particle phase (diameter, density, and the velocity) and the gas phase (viscosity), as well as the configuration of the system, as expressed by the characteristic dimension.

Stk can be considered as a measure of how persistent an airborne particle is when it responds to a sudden change in the velocity and/or direction of the air streamlines. For large *Stk*, it is more difficult for particles to follow the air streamlines faithfully (unlike gas molecules). Particles with large *Stk* will more likely deviate from the air streamlines. When $Stk >> 1$ (high particle inertia), particles continue to travel in a straight line when air changes directions. When $Stk << 1$ (low particle inertia), particles follow the air streamlines perfectly.

In brief, *Stk* is an important parameter to gauge the likelihood of particle deposition due to impaction. For $Stk >> 1$, nearly complete particle losses occur in the sampling system due to high probability of inertial impaction, and vice versa for $Stk << 1$. For *Stk* neither $>>1$ nor $<<1$, the fraction of particle losses due to impaction is a function of *Stk* and the geometrical configuration of the system.†

Figure 4 presents the schematics of sampling inlets with respect to air streamlines and hypothetical particle trajectories under three sampling conditions: (a) isokinetic, (b) sub-isokinetic, and (c) super-isokinetic, with (b) and (c) considered as *anisokinetic* sampling. For example, in the case of ECS air sampling, U_o represents the free-stream air velocity in the ECS duct, and U_{inlet} is the air velocity at the sampling probe. When the sampling is isokinetic ($U_o = U_{inlet}$), aerosols follow the air streamlines and enter the thin-walled sampling inlet with minimum rebound or deposition at the sampling probe entrance. Regardless of particle size and inertia, nearly 100% of particles are collected at the sampling probe entrance under isokinetic sampling, i.e., $\eta_{asp} = 1$.

Sub-isokinetic sampling occurs when $U_{inlet} < U_o$, and this causes air streamlines to decelerate and diverge near the vicinity of the sampling probe inlet. Depending on their inertia, some particles may not make turns as rapidly as air flow streamlines. As a result, particles with certain inertia get into the sampling inlet, which leads to over-sampling ($\eta_{asp} > 1$), as illustrated in Figure 4(b).

On the other hand, in the case of super-isokinetic sampling, $U_{inlet} > U_o$, more air is withdrawn into the inlet. Particles with certain inertia cannot follow the sudden changes of direction and velocity of the air streamlines, and will not be counted in the sampling process ($\eta_{asp} < 1$), as shown in Figure 4(c). Aerosols are under-sampled in this scenario.

The quantitative aspect of sampling deviation owing to anisokinetic sampling will be discussed in Subsection 3.4

---

* By definition, aerosols (or airborne particles) are two-phase systems, consisting of both the particles and gas.

† Usually the estimate of percentage particle loss as a function of *Stk* can be made by experiments and/or numerical modeling.

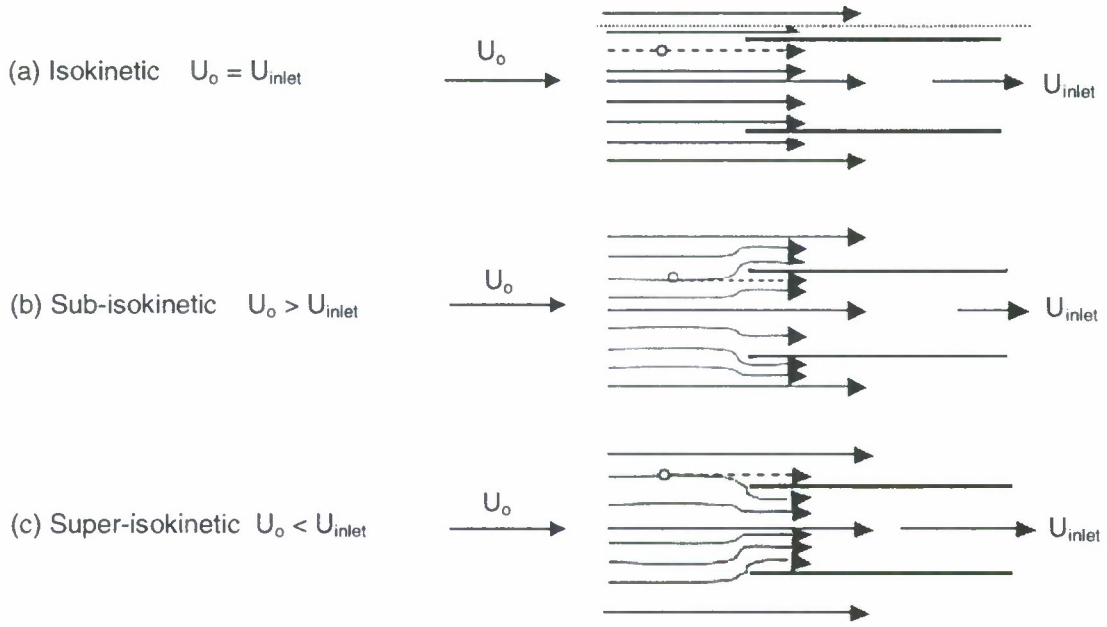

Figure 4. Schematics of sampling inlets with respect to the air streamlines and hypothetical particle trajectories under three sampling conditions: (a) isokinetic; (b) sub-isokinetic, and (c) super-isokinetic. The solid lines represent the air streamlines, and the dotted lines represent the hypothetical particle trajectories that fail to follow air streamlines (when *Stk* >>1), resulting in either over sampling in (b) or under sampling in (c).

3.2 Calculation of an Appropriate Isokinetic Probe I.D.

When the ECS air velocity is changing due to a new flowrate setting and/or change of duct dimensions, a new air velocity associated with the change has to be re-calculated and a *different isokinetic probe* with appropriate inner diameter may be needed (ASTM F25, 1997).

Table 1 is used to illustrate how the appropriate isokinetic probe inner diameter (I.D.) should be determined, and to show the magnitude of the deviation when the sampling is not done isokinetically. Various ECS air flowrates frequently encountered during spacecraft ground operations were examined in this example. Table 1 displays the calculated average air velocities associated with various ECS air flowrates (160, 190, and 300 lb/min) and the duct inner diameters (8, 10, and 12 in.). In order for the average air velocity inside the isokinetic sampling probe to match that in the ECS duct, the appropriate probe I.D. under these scenarios is determined by the following equation:

$$d_1 = d_2\left(\frac{Q_1}{Q_2}\right)^{1/2}, \tag{5}$$

where

d_1: I.D. of an isokinetic probe

d_2: I.D. of an ECS duct

Q_1: sampling probe flowrate, cfm

Q_2: ECS duct air flowrate, cfm

As indicated in Table 1, the average ECS air velocities, U_o, span from 13.8 m/s (160 lb/min air in 12-in. duct) to 58.4 m/s (300 lb/min air in 8-in. duct), and the appropriate isokinetic probe I.D. ranges from 2.8 to 5.8 mm, when air samples are withdrawn to the particle measuring instrument at 1 cfm flowrate.

3.3 Sampling Bias Due to Sampling Probe Thickness

For a thick-walled sampling probe, the presence of the wall thickness causes the distortion of the approaching airflow (See Figure 3), which results in enhanced particle losses at the sampling probe entrance due to particle deposition.

The shape of the sampling probe can greatly affect particle aspiration efficiency.

Figure 5 illustrates the schematic of a sampling probe with the relevant dimensions. According to Belyaev and Levin (1974), a nozzle is considered "thin-walled" when

$D/d \leq 1.1$ regardless of δ/d, β, and Stk; or

$D/d \geq 1.1$ if $\delta/d \leq 0.05$ and $\beta \leq 15°$,

Table 1. Example of Isokinetic Probe I.D. Calculations for a Variety of ECS Airflow Scenarios

	ECS Duct Diameter, inches								
	8			10			12		
Mass flowrate, lb/min	160	190	300	160	190	300	160	190	300
Volumetric flowrate, cfm	2139	2540	4010	2139	2540	4010	2139	2540	4010
Duct avg. air velocity, m/s	31.1	36.9	58.4	19.9	23.7	37.4	13.8	16.4	25.9
Isokinetic probe I.D.*, mm	3.9	3.6	2.8	4.9	4.5	3.6	5.8	5.4	4.3

* Particle counter at sampling flowrate of 1 cfm (28.3 lpm).

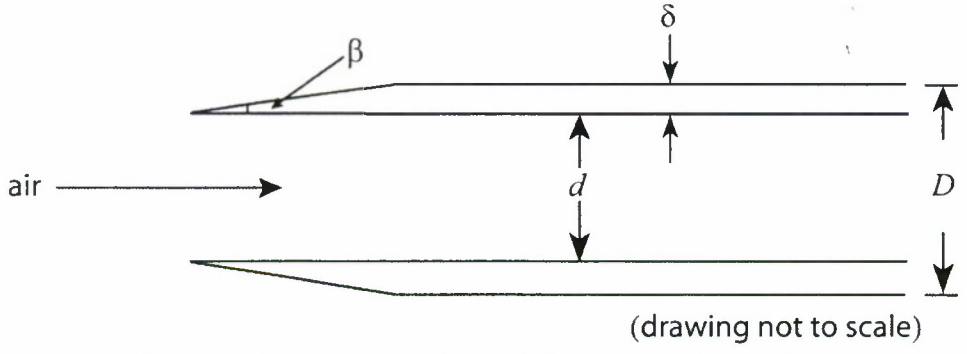

Figure 5. Schematics of a thin-walled aerosol sampling probe.

where

D: isokinetic probe O.D.

d: isokinetic probe I.D.

δ: sampling probe wall thickness

β: tapered angle

The effect of sampling probe wall thickness on the aspiration efficiency, η_{asp}, has been investigated by Belyaev and Levin (1972). Their experimental data suggest that even under isokinetic sampling, η_{asp} could be underestimated by 30–50% when using a thick-walled sampling probe (D/d = 2.5), as compared to using a thin-walled probe (D/d = 1.02).

In addition, Belyaev and Levin (1972) reported on the correlation of aspiration efficiencies on the wall thickness (D/d = 1.02, 1.1, 1.3, 1.7, and 2.5), anisokinetic sampling conditions (U_{inlet}/U_o =0.2, 0.5, 1.0, and 5.0), and the Stokes numbers (Stk = 0.2–3.0). Belyaev and Levin found that η_{asp} decreases significantly with increasing D/d ratios for the same Stk and U_{inlet}/U_o ratios. This information can be used to assess the expected aspiration efficiency when the sampling probe wall is associated with a certain thickness. Examples are shown in Subsection 3.4.

3.4 Estimate of Sampling Deviation due to Anisokinetic Sampling

When airborne particles fail to be collected isokinetically (i.e., anisokinetically), the sampled particle concentration will either overestimate or underestimate the true values, depending on the relative magnitude of gas velocities in sampling probes and in ECS ducts. Such deviations have been quantitatively characterized by both experimental work and numerical calculations where a *thin-walled* probe was employed (Belyaev and Levin, 1974; Liu, *et al.*, 1989).

To illustrate the extent of measurement deviation due to anisokinetic sampling, we assume the use a 0.156-in. I.D. (4 mm) probe at sampling flowrates of 1 and 0.1 cfm, respectively, to sample aerosols at the flowrates and duct diameters indicated in Table 2.

First, as shown in Row (d) of Table 2, the Stokes numbers (Stk) are calculated according to Eq. (4) for 5 μm particles* under each ECS air flow scenario. The Stokes numbers range from 0.27 to 1.15, which means that particle inertia is not negligible, and a fraction of particles will get lost due to impaction at the sampling probe entrance.

Second, when the sampling flowrate is 1 cfm (28.3 L/min), the average air velocity within the sampling probe (4 mm I.D.) is computed as

* 5 μm particles are used for illustration here for their use in FED-STD-209.

Table 2. Calculations of *Stk*, U_{inlet}/U_o, and C_{inlet}/C_o (aspiration efficiency) for a variety of ECS airflow scenarios

	ECS Duct Diameter, Inches								
	8			10			12		
(a) Mass flowrate, lb/min	160	190	300	160	190	300	160	190	300
(b) Volumetric flowrate, cfm	2139	2540	4010	2139	2540	4010	2139	2540	4010
(c) Duct avg. air velocity, m/s	31.1	36.9	58.4	19.9	23.7	37.4	13.8	16.4	25.9
(d) ***Stk* for 5 μm particles**	0.61	0.73	1.15	0.39	0.47	0.74	0.27	0.32	0.51
• For a 4 mm I.D. thin-walled, sharp-edged probe at 1 cfm sampling flowrate[v]									
(e) U_{inlet}/U_o	0.83	0.98	1.56	0.53	0.63	1.0	0.37	0.44	0.69
(f) C_{inlet}/C_o	0.90	0.99	1.43	0.78	0.81	1.0	0.76	0.76	0.83
• For a 4 mm I.D. thick-walled probe (O.D. 0.25") at 1 cfm sampling flowrate[v]									
(g) C_{inlet}/C_o	0.72	0.72	1.14	0.62	0.65	0.8	0.61	0.61	0.66
• For a 4 mm I.D. thin-walled, sharp-edged probe at 0.1 cfm sampling flowrate[¶]									
(h) U_{inlet}/U_o	8.3	9.8	15.6	5.3	6.3	10	3.7	4.4	6.9
(i) C_{inlet}/C_o	6.9	8.5	14.5	3.9	4.9	8.7	2.4	3.0	5.5
(j) ***Stk* for 0.5 μm particles**	0.008	0.0094	0.015	0.0051	0.061	0.0096	0.0035	0.0042	0.0062

[v] the average air velocity within the probe, U_{inlet}, is 37.6 m/s
[¶] the average air velocity within the probe, U_{inlet}, is 3.7 m/s

$$U_{inlet} = \frac{\text{flowrate}}{\text{cross-sectional surface area of sampling probe}}$$

$$= \frac{28.3/1000}{\frac{\pi}{4}(4/1000)^2} \ \frac{\text{m}^3/\text{min}}{\text{m}^2} \times \frac{1}{60} \ \frac{\text{min}}{\text{s}} \qquad (6)$$

$$= 37.6 \text{ m/s}$$

In Row (e), the velocity ratio, U_{inlet}/U_o, is calculated for each duct flow scenario. The particle concentration ratio, C_{inlet}/C_o, also known as aspiration efficiency, η_{asp}, can be estimated based on the following equation (Belyaev and Levin, 1974):

$$\eta_{asp} = \frac{C_{inlet}}{C_o} = 1 + \left(\frac{U_o}{U_{inlet}} - 1\right)\left[1 - \frac{1}{1 + Stk(2 + 0.617U_o/U_{inlet})}\right] \qquad (7)$$

Here, C_{inlet} and C_o refer to the airborne particle concentrations at the sampling probe inlet and in the approaching air streams, respectively.

The goal of isokinetic sampling is to achieve C_{inlet}/C_o close to 1, which means representative aerosol samples are collected into the sampling inlet. Also, keep in mind that the estimate of C_{inlet}/C_o in Eq. (7) is only valid for *thin-walled* sampling probes. As mentioned previously, when a thick-walled probe is involved, the aspiration efficiency or C_{inlet}/C_o values will be always less than 1 even under

isokinetic sampling. Therefore, the C_{inlet}/C_o values in Rows (f) and (i), which were calculated according to Eq. (7), represent the most optimistic estimate for the aspiration efficiency.

With respect to the wall thickness effect, assuming the O.D. of the sampling probe in Table 2 is 0.25 in. (D/d = (0.25 in.)/(0.156 in.) = 1.36), the realistic C_{inlet}/C_o or η_{asp} value for 5 μm particles is estimated to be approximately 0.8 under the isokinetic sampling conditions, according to the results by Belyaev and Levin (1972). In other words, roughly 20% of particles, due to the sampling probe wall thickness effect, are lost right at the very front end of the sampling probe prior to being transmitted through the rest of the sampling system. Therefore, the C_{inlet}/C_o values, assuming D/d = (0.25 in.)/(0.156 in.), will be approximately 20% less than those estimated from a thin-walled sampling probe.

In addition to 1 cfm, the sampling flowrate of 0.1 cfm is sometimes used for collecting ECS air samples in launch ground operations. Therefore, the same calculations were also performed for 0.1 cfm.

The values of U_{inlet}/U_o and C_{inlet}/C_o, as shown in Rows (h) and (i), suggest that when a 4-mm I.D. probe is used for sampling at 0.1 cfm flowrate, one tends to over-estimate the 5-μm particle concentration for all scenarios (sub-isokinetic) by up to a factor of 14.5. Using a thick-walled sampling probe will result in smaller values of C_{inlet}/C_o, but it will still result in over-sampling, thus not a valid measurement.

On the other hand, when a 1-cfm sampling flowrate is employed, there is an underestimate of 5-μm particles for all scenarios (super-isokinetic) except in the case of 300 lb/min air in an 8-in. duct (sub-isokinetic, U_{inlet}/U_o = 1.56).

As shown in Row (j), the Stokes number for 0.5-μm particles were also calculated for all the ECS airflow scenarios in Table 2. Note that all of them are sufficiently small ($Stk << 1$), which means that the particle inertia is negligible. These smaller particles, affected neither by the thick-wall effect nor anisokinetic sampling, can enter the sampling probe inlet at a much higher efficiency than 5 μm and larger particles. Therefore, the aspiration efficiency or C_{inlet}/C_o values for 0.5-μm particles is expected to be close to unity.

For anisokinetic sampling using thin-walled probes, the values of C_{inlet}/C_o have been empirically determined as a function of U_o/U_{inlet} and Stk in experimental studies (Belyaev and Levin, 1974; Durham and Lundgren, 1980) as well as by numerical calculations (Liu, *et al.*, 1989). Both methods showed that the values of C_{inlet}/C_o were in good agreement with each other, and they were well correlated with U_o/U_{inlet} and Stk, as presented in Eq. (7). The predicted aspiration efficiency with respect to anisokinetic sampling, based on Eq. (7), is plotted in Figure 6 for various ratios of U_o/U_{inlet} and Stk.

Figure 6 shows that when $Stk < 0.01$ (e.g., 0.5-μm particles in the scenarios of Table 2), the anisokinetic sampling loss is negligible, thus the aspiration efficiency or C_{inlet}/C_o is very close to 100%. This is due to the fact that particles with sufficiently small inertia can always accommodate the sudden change of airflow in the streamlines and make their way into the sampling probe inlet. At large Stokes numbers, however, the aspiration efficiency (or C_{inlet}/C_o) appears to approach the limiting value of U_o/U_{inlet} based on Eq. (7).

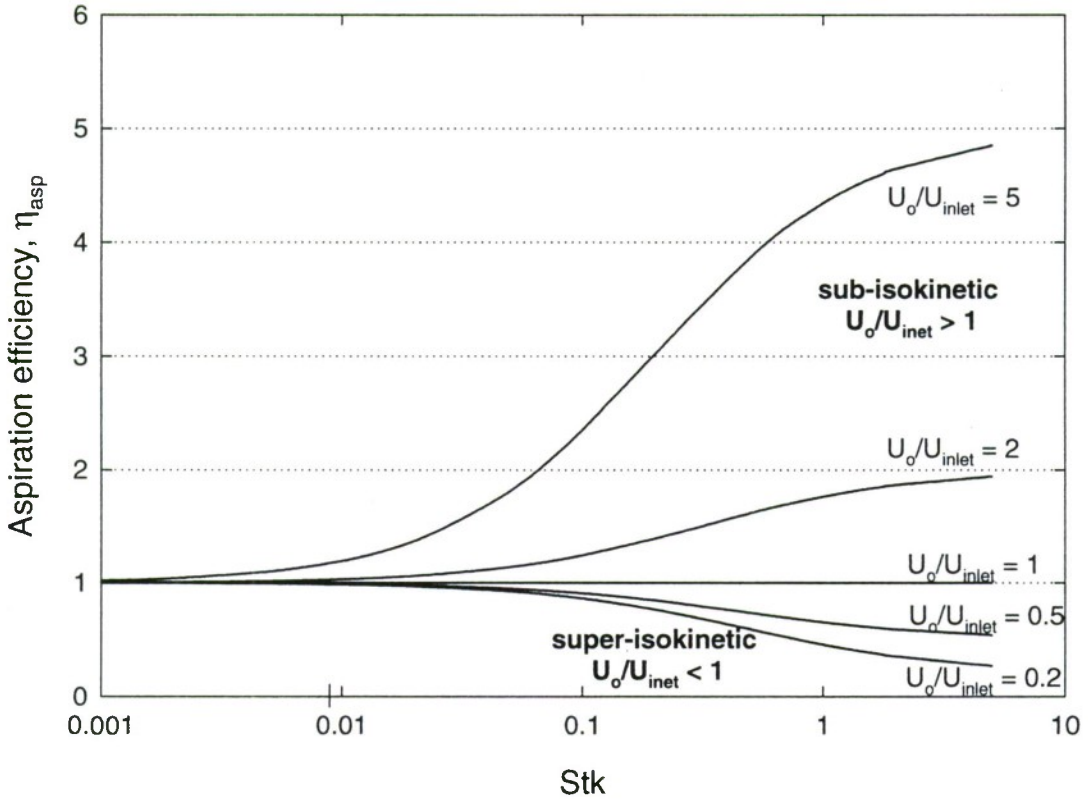

Figure 6. Aspiration efficiency (C_{inlet}/C_o) as a function of the Stokes number (Stk) under various sub-isokinetic and super-isokinetic sampling scenarios using a thin-walled isokinetic probe, which is well aligned with the approaching air streams (inclination angle $\theta = 0°$).

3.5 Summary

Particle aspiration efficiency at the sampling probe strongly depends on the Stokes number (Stk), the airstream velocity ratio (U_o/U_{inlet}), and sampling probe shape/geometry (assuming the probe is well aligned with the incoming air flow). In this section, the air velocities relevant to the likely scenarios of the ECS air quality verification during launch processing are considered. The sample calculations in Tables 1 and 2 on ECS air sampling demonstrate:

1. The combination of a 4-mm (0.156 in.) I.D. probe and 0.1 cfm sampling flowrate does not constitute an isokinetic sampling in any of the cases illustrated in Table 2.

2. The combination of a 4-mm probe and 1 cfm flowrate can sample isokinetically only for the scenarios of 190 lb/min air in an 8-in. duct, and 300 lb/min air in a 10-in. duct.

3. When there is a change in ECS air flowrate or/and ECS duct diameter, the new average air velocity must be re-calculated, and a different isokinetic probe with matching air velocity might be needed to ensure that representative samples are collected.

4. The aspiration efficiency (η_{asp}) decreases with the increasing sampling probe wall thickness for 5-μm particles, which possess sufficient inertia upon entering the sampling probe

for them to be lost. For 0.5-μm particles, on the other hand, the wall thickness effect is not as pronounced, and they are aspirated to the sampling probe at nearly 100% efficiency.

Particle concentrations received at the particle counter tend to be less than the actual particle concentration because of particle losses within the sampling probe, as well as inside the sample transfer line. The losses associated with the sample transfer line are addressed in the next section.

4. Particle Losses Associated with Sampling Lines

4.1 Particle Deposition Mechanisms in Sampling Lines

As mentioned in Section 2, airborne particles are lost not only within the sampling probe but also in the sample transfer line during sampling processes. The extent of particle losses in sampling lines is generally governed by particle size, length, and I.D. of the sampling line and the sampling flowrate.

During transport through the sampling lines, airborne particles can be lost by various deposition mechanisms. The ones commonly encountered during the air sampling procedure are briefly described below.

1. Gravitational settling: particles settle from the moving airstreams under the influence of gravity. They deposit on the lower wall of nonvertical surfaces in a sample transfer line.

2. Diffusional deposition: In still air, small airborne particles are constantly bombarded by their surrounding gas molecules, resulting in the characteristic random motions described as "Brownian diffusion." When there is significant air current involved, such as in the case of 1 cfm sampled air through a sample transfer line, convection or eddy diffusion is responsible for moving small airborne particles toward surfaces. Airborne particles are lost from air once they diffuse toward a wall and deposit on wall surfaces.

3. Turbulent inertial deposition: turbulent flow has been observed to enhance particle deposition in experimental studies. When particle inertia is sufficiently large, there is a high tendency that particles in turbulent flow will move across the air streamlines, penetrate through the boundary layer adjacent to a surface, and eventually deposit on the walls of the sampling line.

4. Inertial deposition at a bend: the trajectory of airborne particles may deviate from the air streamlines owing to their inertia when the direction of sampling air flow is diverted in a bend.

5. Inertial deposition in flow constrictions: particles with sufficiently high inertia will deviate from the air streamlines and collide on the tubing surfaces when air flow contracts or expands abruptly. The resulting particle loss is sometimes difficult to characterize. Estimates for particle transport through flow constrictions can be made in some cases, and these have been made in both numerical and experimental studies.

Figure 7 provides the schematic illustrations of the particle deposition mechanisms mentioned above.

(1) Gravitational settling

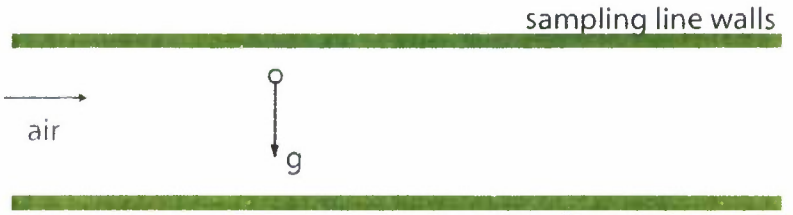

(2) Diffusional deposition

(3) Turbulent inertial deposition

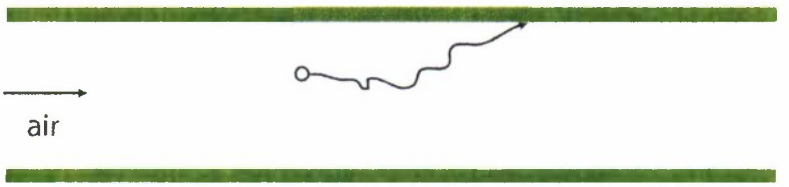

(4) Inertial deposition at a bend

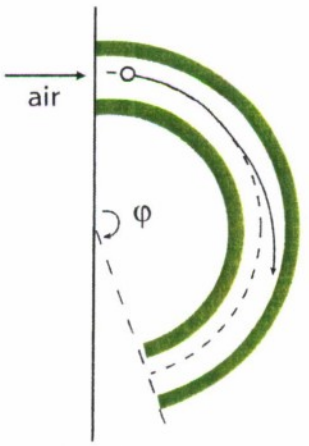

(5) Inertial deposition in flow contrictions

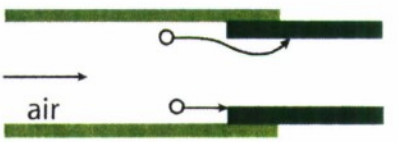

Figure 7. Illustrated particle deposition mechanisms in sampling lines.

When the particles and/or the sampling line are electrically charged, additional particle loss can occur as a result of electrostatic effects. Particle deposition by means of electrostatic effects can be negligible if metal or conductive sampling tubes are used for particle sampling.

4.2 Calculation of Transmission Efficiency in Sampling Lines

A significant body of research on particle depositional loss in conduits and pipes has been performed mainly to understand aerosol transport efficiencies in sampling lines leading to particle detection devices, or the extent of particle penetration into building ventilation ducts, for example. When particles are lost in airstreams due to deposition in an aerosol transport system, the following terminologies are commonly seen and can be used interchangeably.

Transmission efficiency

= transport efficiency

= penetration efficiency

= 1- % particle losses

In this report, we consistently use transmission efficiency along with the subscript (i.e., $\eta_{trans,line}$ for transmission efficiency in a sampling line) to denote the associated elements of the sampling system to avoid confusion.

To reiterate, $\eta_{trans,line}$ is governed by the particle size, and the I.D. and length of the sampling line, as well as the air flow rate. The sampling line orientation with respect to gravity and the degree of sampling line bending also play a role in determining $\eta_{trans,line}$. Correlations evaluating $\eta_{trans,line}$ associated with the above parameters in aerosol sampling lines of circular cross section are summarized in Table 3. As indicated in Table 3, the equations are categorized according to the various particle deposition mechanisms under laminar and turbulent flow regimes.[7] The Reynolds number (Re) can be used to characterize the degree of air turbulence in various flow systems, and here in the example of aerosol sampling lines, Re is given by

$$\mathrm{Re} = \frac{UD_{tube}}{\nu}, \tag{8}$$

where

U: average air flow velocity in the sampling line

D_{tube}: internal diameter of the sampling line

ν: kinematic air viscosity; 1.5×10^{-5} m^2/s at 20°C.

[7] As a note, the correlations for laminar flow conditions in Table 3 were obtained by setting up the governing equations for air (Navier-Stokes equation and continuity equation) and for particle transport (equations of motion), and then solving them simultaneously. The correlations for turbulent flow conditions were empirically formulated. Both types of correlations have been validated by experiments, as seen in the references shown in Table 3.

By convention, Re ≤ 2000 is considered as laminar flow conditions, and Re ≥ 3000 is classified as turbulent flow regimes in a duct/pipe system (also known as "internal flow" systems). Note that the correlations in Table 3 may not apply to transition flow regimes (2000 ≤ Re ≤ 3000) because the fluid flow is highly unpredictable and often changes between laminar and turbulent states.

In the case of particle transport at 1 cfm (28.3 lpm) through a sampling line with an example tubing I.D. of 0.375 in. (9.53 mm; used for on-pad ECS air sampling), the average air velocity within the sampling line is:

$$U = \frac{\text{flowrate}}{\text{cross}-\text{sectional surface area of sampling probe}}$$

$$= \frac{28.3\times 1000}{\frac{\pi}{4}(0.953)^2}\frac{cm^3/\min}{cm^2}\times\frac{1}{100}\frac{m}{cm}\times\frac{1}{60}\frac{\min}{s}$$

$$= 6.62 m/s$$

Re is then calculated as:

$$\mathrm{Re} = \frac{UD_{tube}}{\nu} = \frac{6.62 m/s \cdot 0.00953 m}{1.5\cdot 10^{-5} m^2/s} \sim 4200.$$

The air flow within the sampling line is thus characterized as turbulent flow.

The total particle transmission efficiency associated with the sampling line, $\eta_{trans,line}$, is the product of the transmission efficiencies with respect to each deposition mechanism in each flow element (laminar or turbulent). For example, in turbulent flow,

$$\eta_{trans,line,turb} = \eta_{grav,turb} \times \eta_{diff,turb} \times \eta_{inert,turb} \times \ldots \quad (9)$$

or in laminar flow,

$$\eta_{trans,line,lam} = \eta_{grav,lam} \times \eta_{diff,lam} \times \eta_{inert,lam} \times \ldots \quad (10)$$

The Appendix provides the details of example particle transmission efficiency calculations. Although the air within the sampling line belongs to the turbulent flow regime in the ECS air sampling procedure, formulas used in the laminar flow regime are also provided for calculating $\eta_{trans,line}$ for future references.

Table 3. Correlations Used for Calculating Particle Transmission Efficiency for Various Particle Deposition Mechanisms in Circular Sampling Lines

	Turbulent Flow	Laminar Flow
Gravitational settling	$\eta_{grav,turb} = \exp\left[-\frac{dLV_S\cos\theta}{Q}\right]$ V_s: particle settling velocity Q: sampling flowrate θ: the angle of inclination with respect to the horizontal component. Schwendiman *et al.* (1975)	$\eta_{grav,lam} = 1-\frac{2}{\pi}\left[2\varepsilon\sqrt{1-\varepsilon^{2/3}} - \varepsilon^{1/3}\sqrt{1-\varepsilon^{2/3}} + \arcsin\left(\varepsilon^{1/3}\right)\right]$ $\varepsilon = \frac{3LV_S}{dU}\cos\theta$ Fuch (1964); Pich (1972)
Diffusion	$\eta_{diff,turb} = \exp\left[-\frac{\pi DL}{Q}Sh\right]$ Friedlander (1977) Sh: Sherwood number; $= 0.0118\,\mathrm{Re}_f^{\,7/8}\,Sc^{1/3}$ Re_f: Reynolds number in fluid; $= \rho_f Ud/\mu$ Sc: Schmidt number; $= \mu/\rho_f D$ D: particle diffusion coefficient d: tubing I.D. L: tubing length	$\eta_{diff,lam} = 1-2.56\xi^{2/3}+1.2\xi+0.177\xi^{3/4}$ for $\xi < 0.02$ $\eta_{diff,lam} = 0.819\exp(-3.657\xi)+0.097\exp(-22.3\xi)+0.032\exp(-57\xi)$ for $\xi > 0.02$ $\xi = \frac{\pi DL}{Q}$ Gormley and Kennedy (1949)
Turbulent inertial deposition	$\eta_{inert,turb} = \exp\left[-\frac{\pi dLV_t}{Q}\right]$ $V_t = V_+\frac{U}{5.03}\mathrm{Re}_f^{-1/8}$; deposition velocity for turbulent inertial deposition V_+: dimensionless deposition velocity;	not applicable in laminar flow

	$\tau_+ = 0.0395 Stk \, \mathrm{Re}_f^{3/4}$; dimensionless particle relaxation time Lee and Gieseke (1994)	
Inertial deposition in a bend	$\eta_{inert,bend,turb} = \exp[-2.823 Stk \varphi]$ φ: the angle of the bend in radians Pui *et al.* (1987)	$\eta_{inert,bend,lam} = 1 - Stk\varphi$ Crane and Evans (1977) φ: the angle of the bend in radians
Inertial deposition in flow constrictions	$\eta_{inert,cont,turb} = 1 - \frac{1}{1 + \left\{ \frac{2Stk\left[1 - \left(\frac{d_l}{d_s}\right)^2\right]}{3.14\exp(-0.0185\theta)} \right\}^{-1.24}}$ θ: the contraction angle in degrees d_l: I.D. of a larger diameter tube d_s: I.D. of a smaller diameter tube *Stk*: based on the small-diameter tube and average velocity in the large tube Muyshondt *et al.* (1996)	$\eta_{inert,cont,lam} = 1 - \left[1 - \left(\frac{d_l}{d_s}\right)^2\right]^2$ Chen and Pui (1995)

Based on the equations summarized in Table 3, one can evaluate the particle transmission efficiency at any given sampling tube I.D., length, bending conditions, and the sampling flowrate. Figure 8 presents the calculated total particle transmission efficiency in the sampling line as a function of particle size under various tubing configurations, which are all assumed to be in horizontal orientations. In addition, the estimate of particle loss due to flow constrictions is applied to the connection of the sampling line and the inlet of a particle counter (see Appendix for details).

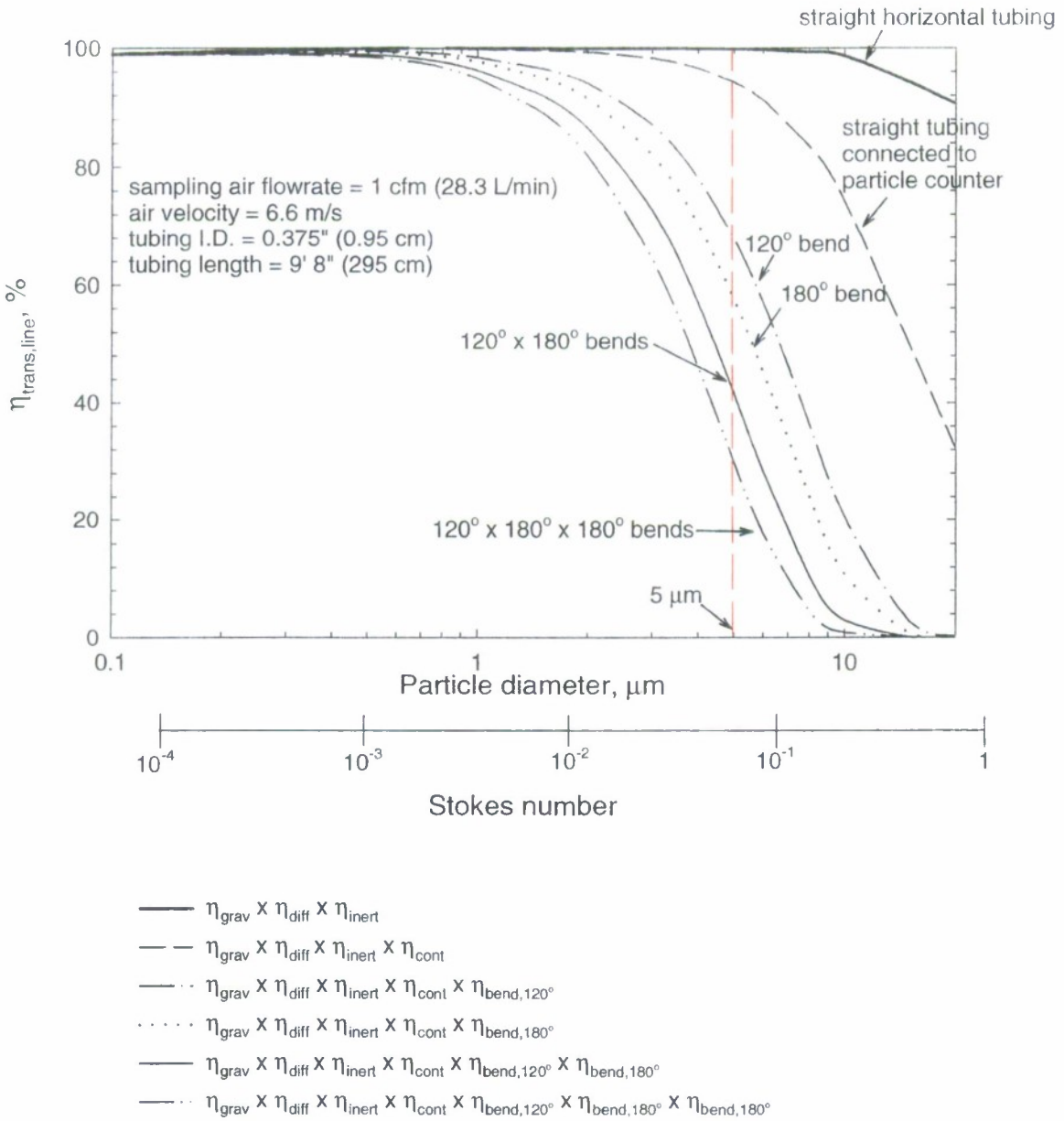

Figure 8. Calculated transmission efficiencies with respect to the sampling line, $\eta_{tran,line}$, as functions of the particle diameter and the Stokes number under various tubing configurations. The sampling flowrate is 1 cfm.

From Figure 8, it is clear that bends in a sampling line play a key role in determining the particle transmission efficiency.* High transmission efficiency means little particle loss in the line. For a 5-μm particle, for example, the estimated transmission efficiency drops from 94% in a straight horizontal tubing to 68% with one 120° bend, and 58% with one 180° bend, respectively. When more bends are involved in the tubing, more particles are lost at bends due to inertial impaction, which, in turn, results in even lower transmission efficiency. As indicated in Figure 8, the particle transmission efficiencies are estimated to be 42% and 30% for the existence of 2 bends (120° and 180°) and 3 bends (120°, 180° and 180°), respectively.

On the other hand, the transmission efficiency for 0.5-μm particles ($Stk << 0.01$ in the sampling line) is estimated to be nearly 100%, meaning very little particle loss within the sampling line.

4.3 Calculation of Transmission Efficiency within a Sampling Probe

When the sampling probe has a substantial length, one can apply the above calculations to estimate particle transmission efficiency associated with a sampling probe, namely, the fraction of aspirated particles that are transmitted through the inlet to the rest of the sampling system.

For example, when the sampling probe I.D. is 0.156 in. (0.4 cm), the length is 1.5 ft (45.7 cm), and with one 180° bend (as shown in Figure 9), the calculated transmission efficiency contributed from various deposition mechanisms is presented in Figure 10.

As shown in Figure 10, the 180° bend of the sampling probe has the detrimental effect of losing all particles of 5 μm and above. Note that the Stokes number for 5-μm particles is close to 1, which means particle inertia under this flow condition becomes non-negligible. Therefore particles of 5 μm in diameter and greater have a high likelihood of getting lost inside the sampling probe by means of inertial deposition. The transmission efficiency shows slight improvements when the bend is 90°, but it is still less than 5% for 5 μm particles.

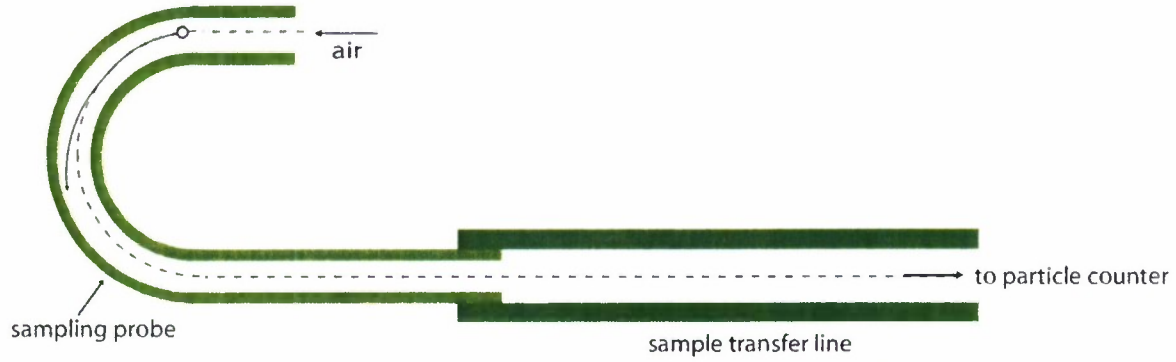

Figure 9. A postulated aerosol sampling probe (not to scale)

* In FED-STD-209E, the statement of "For particles in the range of 2–10 μm the transit tube should be no longer than 3 m." referred in B40.2.1 is only true when no bends are involved in the transit tube (sampling line).

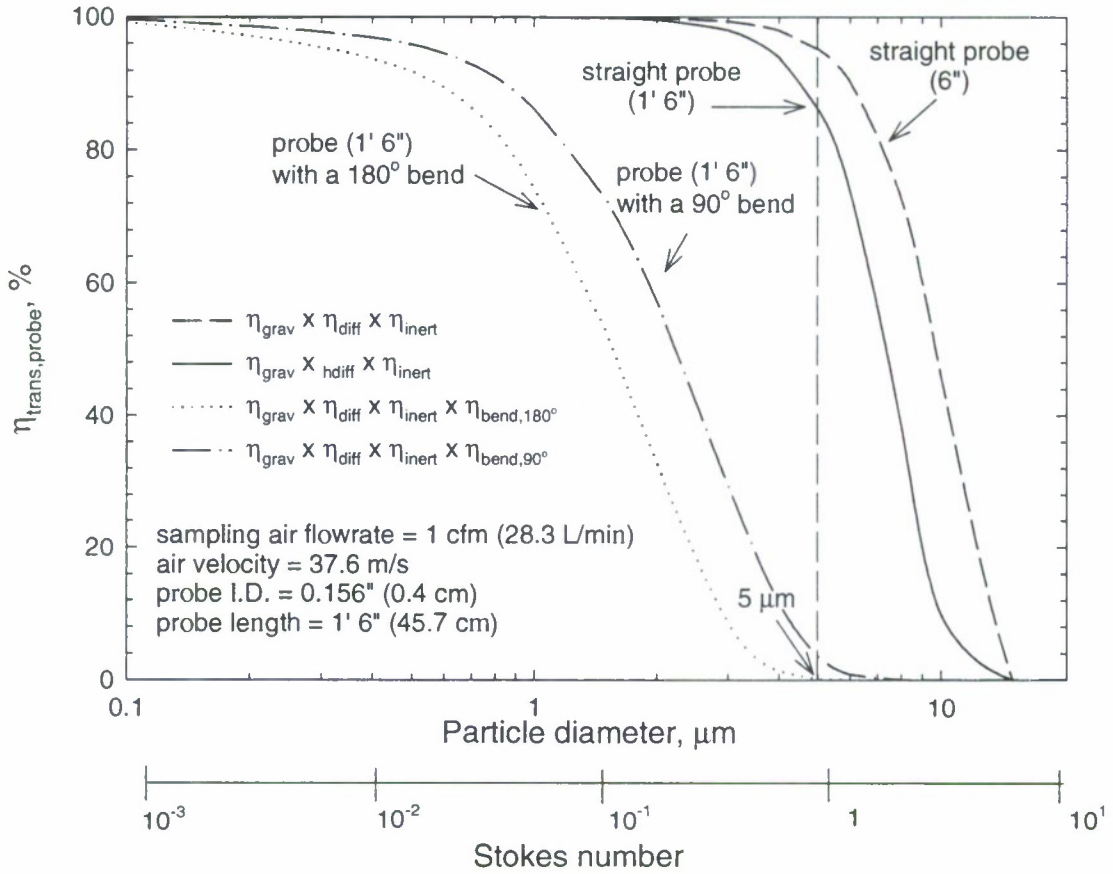

Figure 10. Calculated transmission efficiencies with respect to the sampling probe, $\eta_{tran,probe}$, as a function of particle diameters and the Stokes number associated with the sampling probe with the characteristics illustrated in Figure 9.

When the sampling probe is set straight with the identical length (1.5 ft; 45.7 cm), the transmission efficiency rises up to 86% for 5-µm particles. As shown in Figure 10, the transmission efficiency can be significantly improved if the sampling probe length can be further reduced; e.g., 95% transmission efficiency for 6-in. (15.2 cm) probe length.

In this sample calculation, the Stokes numbers of particles in the sampling probe are one order of magnitude higher than those in the sampling line (due to higher air velocity resulting from smaller probe I.D. at identical flowrate of 1 cfm); therefore, particle losses as a result of inertial deposition at the bends and wall surfaces become more pronounced within the probe as compared with the sampling line. For sufficiently high *Stk*, reducing probe length and avoiding bends will help minimize particle losses due to turbulent inertial deposition.

4.4 Summary

Assuming aerosol sampling is done isokinetically with a thin-walled probe ($\eta_{asp} \sim 1$), the particle concentration received at the particle measurement device will be lower than the particle concentration aspirated at the sampling probe inlet because particles are inevitably lost during transmission in

the sampling system. In the case study demonstrated in this section, we have selected the sampling line and probe with the geometries and air sampling flowrate relevant to the routine ECS air quality verification procedures in launch processing operations. As shown in the calculations, 5-μm particles and larger can be subject to significant loss owing to inertial deposition. The loss is enhanced when the sampling line and probe are designed with bends. On the other hand, 0.5-μm particles have much higher transmission efficiency because they do not get lost easily within the sampling line due to their negligible inertia. Therefore, the particle counts measured in this size range would better represent the actual particle concentration associated with that size range in the fast-moving ECS air.

5. Recommendations for ECS Air Quality Testing

Prior to connection of the ECS air to payload fairing, the airborne particle concentrations from the ECS air must be verified to ensure that the air cleanliness level meets the mission specifications, for instance, Class 5000 with the goal of Class 100* per FED-STD-209E. This report has quantitatively examined the aerosol sampling errors associated with the ECS air cleanliness verification process during launch site ground operations.

The following guidelines will help collecting airborne particles with minimal sampling losses inside the ECS duct:

1. A *thin-walled*, isokinetic probe should be inserted at the center of the ECS duct and at least 6 in. *inside* the duct end.
2. The sampling probe must be well aligned with the incoming air streams.
3. Avoid bends in the sampling system. If a sample transfer line must contain bends prior to connecting to a particle counter, a large and gradual turn of the tubing is strongly recommended. Abrupt turns should be avoided to minimize particle losses due to inertial impaction in the transfer line.
4. A sample transfer line should be kept as short as possible to minimize particle losses due to gravity, diffusion, and inertial deposition in the tubing. Particle size, tubing I.D., tubing length, and the air velocity all play a role in determining the extent of particle losses during the sample transport process.
5. Use conductive sampling inlets and sampling lines. Teflon and Polyflo should be avoided for aerosol sampling owing to potential enhanced particle deposition by electrostatic forces (Liu *et al.*, 1985).

* Especially for optical payloads.

6. Conclusions

Sampling of airborne particles from the fast-moving ECS air is a challenging task. Collecting a representative aerosol sample requires taking into account the relative magnitude of air velocities at the sampling inlet and in the free-stream air, the alignment of the sampling probe to the free-stream air, and the sampling probe shape and geometry, as well as particle inertia. Analysis in this report demonstrates that one sampling probe appropriate to sample airborne particles in one ECS air duct flow scenario may not be suitable otherwise. One can run a quick calculation of the expected new duct air velocity and determine whether a sampling probe of a different I.D. is required in order to sample particles isokinetically. In this report, several representative ECS air flowrates under various duct dimensions were illustrated in the case studies, and the expected deviations from true representation of ECS air as a result of anisokinetic sampling and sampling probe wall thickness were examined.

Once aerosols are withdrawn into the sampling probe, particle losses should be minimized during sample transmission by avoiding unnecessary lengths and bends. Particle transmission efficiency is a function of particle size, and sampling line I.D. and length, as well as sampling flowrate. In the sample calculations, we have selected the representative sampling tubing length and I.D. routinely used for ECS air quality verification in launch processing operations. The particle transmission efficiencies associated with various sampling line bending arrangements were evaluated based on empirical equations published in the existing literature, as compiled in Table 3. The calculations have shown that under the high air velocities in the sampling system, a bend will cause significant particle losses for 5-μm and larger particles.

Summarized from the calculations demonstrated in previous sections, Table 4 presents the estimated overall transmission efficiencies for 5-μm and larger particles, starting at the sampling probe entrance through the sampling line to the particle counter inlet, for various probe and tubing configurations under the following sampling conditions:

1. Isokinetic sampling with the probe wall thickness effect (D/d = O.D./I.D. = (0.25 in.)/(0.156 in.) = 1.36) yields η_{asp} of 0.8.
2. The sampling probe length is 1.5 ft, and it is assumed to be horizontal and straight, or have at most one bend with the angle noted in Table 4.
3. The I.D. and length of the sampling line are 0.375 in. and 9.67 ft, respectively. The sampling line is assumed to have one to three bends as shown in Table 4.
4. The sampling flowrate is 1cfm.

As suggested in Eq. (1), the overall transmission efficiency of the sampling system is computed as the product from the following three elements:

$$\eta_{\text{overall}} = \eta_{asp} \times \eta_{trans.probe} \times \eta_{trans,line} \quad (1)$$

Table 4. Summary of the Calculated Overall Transmission Efficiencies for 5-μm Particles in the Sampling System*

Aspiration efficiency (η_{asp})	Sampling probe (# of bends and angle)	Transmission efficiency for sampling probe ($\eta_{trans,probe}$)	Sampling line (# of bends and angle)	Transmission efficiency for sampling line ($\eta_{trans,line}$)	Overall transmission efficiency ($\eta_{overall}$)
0.8	no bend	0.86	no bend	0.94	0.65
0.8	1, 90°	0.04	no bend	0.94	0.03
0.8	1, 180°	0	no bend	0.94	0.00
0.8	no bend	0.86	1, 120°	0.68	0.47
0.8	no bend	0.86	1, 180°	0.58	0.40
0.8	no bend	0.86	2, 120° x 180°	0.42	0.29
0.8	no bend	0.86	3, 120° x 180° x 180°	0.30	0.21
0.8	1, 90°	0.04	1, 120°	0.68	0.02
0.8	1, 90°	0.04	1, 180°	0.58	0.02
0.8	1, 90°	0.04	2, 120° x 180°	0.42	0.01
0.8	1, 90°	0.04	3, 120° x 180° x 180°	0.30	0.01

*assuming isokinetic sampling; sampling probe O.D. and I.D. are 0.25" and 0.156", respectively; sampling probe length is 1'6"; sampling line I.D. is 0.375" and sampling line length is 9'8"; sampling flowrate is 1 cfm.

The postulated scenarios in Table 4 are selected to simulate the major characteristics of the sampling system for ECS air verification and to provide indications with respect to the expected particle transmission efficiency associated with the different practice of the sampling procedures. As shown in Table 4, the overall transmission efficiency of 5-μm particles or larger is low for sampling configurations routinely used for ECS air cleanliness verification. In typical ECS air cleanliness measurements taken so far, the vast majority of counts in this size range are either zero or one. For counts this small, there are two possible interpretations based on the calculations in Table 4:

(1) The actual count of 5-μm particles and larger could be as high as 98 or 99 (for 0.01–0.02 transmission efficiency), but the particle counter sees zero or one particle due to losses in the sampling system.

or

(2) The air might actually contain zero or one particle per cubic foot of air (as in the case of a well-functioned ECS), thus there are no particles to be lost.

Table 4 provides useful information to assess the likely true aerosol concentrations when the particle counts in the free air streams are above or near the requirement limit, such as 35 per cubic foot for Class 5000 per FED-STD-209E. In such cases, particle losses in the sampling systems must be considered.

On the other hand, the measurement of 0.5-μm particles serves a better indicator for the purge air quality verification owing to nearly 100% transmission efficiency for this particle size range. An

improved design for sampling 5-μm and larger particles with minimal sampling losses would be highly desirable to provide valid data, which can be used to diagnose the ECS anomalies before spacecraft are exposed to contamination risks.

References

ASTM F25, Isokinetic sampling of a moving gas stream in a duct or pipeline, Appendix X1, Vol. 15.03, 1997.

Baron, P. A. and Willeke, K. *Aerosol Measurement — Principles, Techniques, and Applications*, 2001, 2nd edition, John Wiley & Sons.

Belyaev, S. P., Levin, L. M., Investigation of aerosol Aspiration by photographing particle tracks under flash illumination, *Journal of Aerosol Science*, 1972, 3: 127-140.

Belyaev, S. P., Levin, L. M., Techniques for collection of representative aerosol samples, *Journal of Aerosol Science*, 1974, 5: 325-338.

Chen, D.-R. and Pui, D. Y. H., Numerical and experimental studies of particles deposition in a tube with conical contraction — Laminar flow regime, *Journal of Aerosol Science*, 1995, 26: 563-574

Crane, R. L., and Evans, R. L., Inertial deposition of particles in a bent pipe, *Journal of Aerosol Science*, 1977, 8:161-170.

Durham, M. D., and Lundgren, D. A. Evaluation of aerosol aspiration efficiency as a function of Stokes number, velocity ratio and nozzle angle, *Journal of Aerosol Science*, 1980, 11:179-188.

FED-STD-209E, *Federal Standard: Airborne Particulate Cleanliness Classes in Cleanrooms and Clean Zones*, Appendix C, 1992.

Friedlander, S. K., *Smoke, Dust, and Haze*, 1977, John Wiley & Sons.

Gromley, P. G., and Kennedy, M., Diffusion from a stream flowing through a cylindrical tube, *Proc. R. Irish Academy*, 1949, 52A:163-169.

Hinds, W. C., *Aerosol Technology: Properties, Behavior, and Measurement of Airborne Particles*, 1999, 2nd edition, John Wiley & Sons.

Lee, K. W., and Gieseke, J. A., Deposition of particles in turbulent pipe flows, *Journal of Aerosol Science*, 1994, 26:699-709.

Liu. B. Y. H., Pui, D. Y. H., Rubow, K. L., Szymansky, W. W., Electrostatic effects in aerosol sampling and filtration, *The Annals of Occupational Hygiene*, 1985, 29:251-269.

Liu, B.Y.H., Zhang, Z.Q., Kuehn, T.H., A numerical study of inertial errors in anisokinetic sampling, *Journal of Aerosol Science*, 1989, 20: 367-380.

Muyshondt, A., McFarland, A. R., and Anand, N. K., Deposition of aerosol particles in contraction fittings, *Aerosol Science and Technology*, 1996, 24: 205-216.

Pich, J., Theory of gravitational deposition of particles from laminar flows in channels, 1972, *Journal of Aerosol Science*, 3:351-361.

Pui, D. Y. H., Romay-Novas, F., and Liu, B. Y. H., Experimental study of particle deposition in bends of circular cross section, *Aerosol Science and Technology*, 1987, 7: 301-315.

Schwendiman, L. G., Stegen, G. E., Glissmeyer, J. A., Report BNWL-SA-5138, 1975, Battelle Pacific Northwest Laboratory, Richland, WA.

Appendix—Sample Calculations of Particle Transmission Efficiency in an ECS Air Sampling Line

This appendix demonstrates the procedures for assessing particle transmission efficiency through an example ECS air sampling line. The following sampling line characteristics and a particle of 5 μm diameter (d_p) are used in the calculation:

Tubing I.D., $d = 0.375$ in. = 0.95 cm

Tubing length, $L = 9.67$ ft = 295 cm

Sampling flowrate, $Q = 1$ cfm = 28.3 L/min

Air properties:

assuming air temperature, T = 20°C

air dynamic viscosity, $\mu = 1.8 \times 10^{-5}$ kg/m·s

air kinematic viscosity, $\nu = 1.5 \times 10^{-5}$ m^2/s

air density, $\rho_f = 1.2$ kg/m^3

average air velocity in the sampling line, $U = Q/(1/4)\pi d^2 = 6.62$ m/s

Reynolds number, $Re_f = Ud/\nu = 4200$ (turbulent flow)

Particle properties

assuming particle density, $\rho_p = 1000$ kg/m^3

and particle temperature is very close to air fluid temperature

Stokes number (Stk) of 5 μm particles = $\rho_p d_p^2 U C_c/18\mu d = 0.0055$

Calculations of transport efficiencies by various particle deposition mechanisms:

(1) η_{grav} by gravity

particle settling velocity of a 5 μm particle = $\rho_p d_p^2 g C_c/18\mu = 0.078$ cm/s

$$\eta_{grav} = \exp\left[-\frac{dLV_S \cos\theta}{Q}\right] = 0.999$$

assuming $\theta = 90°$ (vertical tubing; most conservative scenario)

(2) η_{diff} by diffusion

$$\eta_{diff} = \exp\left[-\frac{\pi DL}{Q} Sh\right] = \exp\left[-\frac{\pi DL}{Q}\left(0.0118\,\mathrm{Re}_f{}^{7/8}\left(\frac{\eta}{\rho_f D}\right)^{1/3}\right)\right] = 1$$

where D: particle diffusion coefficient

$$D = \frac{kTC_c}{3\pi\mu d_p}$$

k: Bolzmann's constant; 1.38×10^{-16} dyn·cm/K

T: absolute temperature in K

(3) η_{inert} by turbulent inertial deposition

$$\eta_{inert} = \exp\left[-\frac{\pi dLV_t}{Q}\right]$$

$$= \exp\left[-\frac{\pi dL}{Q}\left(6\times10^{-4}\left(0.0395Stk\,\mathrm{Re}_f{}^{3/4}\right)+2\times10^{-8}\,\mathrm{Re}_f\right)\frac{U}{5.03}\mathrm{Re}_f{}^{-1/8}\right]$$

$$= 0.999$$

(4) $\eta_{inert,\,bend}$ by inertial deposition in a bend

$$\eta_{inert,bend} = \exp[-2.823Stk\varphi]$$

assuming 120° bend ($\varphi = 2\pi/3 = 2.09$)

$$\eta_{inert,bend} = \exp[-2.823 \cdot 0.0055 \cdot 2.09] = 0.722$$

(5) $\eta_{inert,cont}$ **by inertial deposition in flow constrictions**

This is to estimate particle loss resulting from particle entry into the inlet of a particle counter with a smaller I.D (assuming 0.25 in.). The contraction angle (θ) is 90°.

$$\eta_{inert,cont} = 1 - \frac{1}{1 + \left\{ \frac{2Stk\left[1 - \left(\frac{d_1}{d_s}\right)^2\right]}{3.14\exp(-0.0185\theta)} \right\}^{-1.24}}$$

$$= 1 - \frac{1}{1 + \left\{ \frac{2 \cdot 0.0055\left[1 - \left(\frac{0.375}{0.25}\right)^2\right]}{3.14\exp(-0.0185 \cdot 90)} \right\}^{-1.24}}$$

$$= 0.943$$

PHYSICAL SCIENCES LABORATORIES

The Aerospace Corporation functions as an "architect-engineer" for national security programs, specializing in advanced military space systems. The Corporation's Physical Sciences Laboratories support the effective and timely development and operation of national security systems through scientifie research and the application of advanced technology. Vital to the success of the Corporation is the technical staff's wide-ranging expertise and its ability to stay abreast of new technological developments and program support issues associated with rapidly evolving space systems. Contributing capabilities are provided by these individual organizations:

Electronics and Photonics Laboratory: Microelectronics, VLSI reliability, failure analysis, solid-state device physics, compound semiconductors, radiation effects, infrared and CCD detector devices, data storage and display technologies; lasers and electro-optics, solid-state laser design, micro-optics, optical communications, and fiber-optic sensors; atomic frequency standards, applied laser spectroscopy, laser chemistry, atmospheric propagation and beam control, LIDAR/LADAR remote sensing; solar cell and array testing and evaluation, battery electrochemistry, battery testing and evaluation.

Space Materials Laboratory: Evaluation and characterizations of new materials and processing techniques: metals, alloys, ceramics, polymers, thin films, and composites; development of advaneed deposition proeesses; nondestruetive evaluation, component failure analysis and reliability; structural mechanics, fracture mechanics, and stress eorrosion; analysis and evaluation of materials at cryogenic and elevated temperatures; launch vehicle fluid mechanics, heat transfer and flight dynamies; aerothermodynamics; chemical and electric propulsion; environmental chemistry; combustion processes; space environment effects on materials, hardening and vulnerability assessment; contamination, thermal and structural control; lubrication and surface phenomena. Microelectromechanical systems (MEMS) for space applications; laser micromachining; laser-surface physical and chemical interactions; micropropulsion; micro- and nanosatellite mission analysis; intelligent microinstruments for monitoring spaee and launeh system environments.

Space Science Applications Laboratory: Magnetospheric, auroral and cosmie-ray physies, wave-particle interactions, magnetospheric plasma waves; atmospheric and ionospheric physics, density and composition of the upper atmosphere, remote sensing using atmospheric radiation; solar physics, infrared astronomy, infrared signature analysis; infrared surveillance, imaging and remote sensing, multispectral and hyperspectral sensor development; data analysis and algorithm development; applications of multispectral and hyperspectral imagery to defense, civil space, eommercial, and environmental missions; effects of solar activity, magnetic storms and nuclear explosions on the Earth's atmosphere, ionosphere and magnetosphere; effects of electromagnetic and particulate radiations on space systems; space instrumentation, design, fabrication and test; environmental chemistry, trace detection; atmospherie chemical reactions, atmospheric optics, light scattering, state-specific chemical reactions, and radiative signatures of missile plumes.